Experimental Observation of Quantum Holographic Imaging

Xin-Bing Song,[1] De-Qin Xu,[1] Hai-Bo Wang,[1] Jun Xiong,[1]
Xiangdong Zhang,[1] De-Zhong Cao,[2] and Kaige Wang[1,*]

[1]*Department of Physics, Applied Optics Beijing Area Major Laboratory, Beijing Normal University, Beijing 100875, China*

[2]*Department of Physics, Yantai University, Yantai 264005, China*

Abstract

We report the first experimental observation of quantum holographic imaging with entangled photon pairs, generated in a spontaneous parametric down-conversion process. The signal photons play both roles of "object wave" and "reference wave" in holography but are recorded by a point detector providing only encoding information, while the idler photons travel freely and are locally manipulated with spatial resolution. The holographic image is formed by the two-photon correlation measurement, although both the signal and idler beams are incoherent. According to the detection regime of the signal photons, we analyze three types of quantum holography schemes: point detection, coherent detection and bucket detection, which can correspond to classical holography using a point source, a plane-wave coherent source and a spatially incoherent source, respectively. Our experiment demonstrates that the two-photon holography in the point detection regime is equivalent to the one-photon holography using a point source. Physically, the quantum holography experiment verifies that a pair of non-commutable physical quantities, the amplitude and phase components of the field operator, can be nonlocally measured through two-photon entanglement.

*Author to whom correspondence should be addressed:wangkg@bnu.edu.cn

Holography, first proposed by Gabor in 1948[1], is a lensless imaging technique and capable of recording entire information of an object. Different from usual photography, where only the intensity of the optical field shining an object is recorded, both the amplitude and phase of the field are recorded by adding a reference field in holography. Hence holography requires a coherent source with both better temporal and spatial coherence, such as a laser beam, to perform the spatial interference between the object wave and reference wave. A challenging question would be: can holography be performed by other sources, which are not coherent or even nonclassical? Recently, Zhang et al.[2, 3] discovered that the spatial coherence is not necessary in the holographic interference. Their schemes used an incoherent thermal light source with an extended area, and the object wave and reference wave are arranged to experience different diffraction configurations. Different from coherent holography where the holographic pattern is stationary, the interference pattern in the incoherent regime fluctuates in time, but can be formed in the statistical summation.

Spontaneous parametric down-conversion (SPDC) process in a nonlinear crystal may generate a nonclassical light source - the two-photon quantum entangled state, which is very close to the Einstein-Podolsky-Rosen (EPR) state[4]. The two down-converted beams in SPDC are incoherent, but the coherence can be revived in the two-photon correlation. In the pioneer theoretical work of two-photon optics, Belinskii and Klyshko[5] predicted three spooky schemes: two-photon diffraction, two-photon holography, and two-photon transformation of two-dimensional images. The first and last schemes have been demonstrated in the experiments, known as ghost interference[6] and ghost imaging[7], respectively. These experiments were regarded as close to the original *gedankenexperiment* of EPR paradox, since the position or momentum information detected by one photon can be nonlocally transferred to the other photon. However, to our best knowledge, the two-photon holography has not been tested experimentally so far.

In 2001, Abouraddy et al [8] proposed a theoretical scheme of quantum holography using a two-photon entangled source. In their scheme, one photon of the entangled photon pair illuminates the remote object and then is collected by a bucket detector while the other is locally manipulated providing conventional spatial resolution. Since quantum entanglement behaves as “spooky actions at a distance” (in Einstein’s word)[9], the holographic information of the remote object can be recorded by the coincidence measurement of the two photons. They claimed that quantum holography is particularly suitable for imaging of a

hidden object or an object in a confined space where the conventional imaging is impossible. Later, they realized the entangled-photon ghost imaging experiment with a pure phase object, but not holographic imaging[10].

In this paper, we report the first experimental observation of holographic imaging using a two-photon entangled source. In our detailed theoretical analysis, we find that the quantum holography scheme in terms of bucket detection proposed by Abouraddy et al [8] is restricted in the experimental performance. We compare two different detection regimes in the two-photon quantum holography, the bucket detection and the point detection, both of which record the encoding information of the photon shining the object. As a matter of fact, quantum holography fails if the bucket detection is applied to the holographic interference where the two interfered waves experience the same diffraction length. However, the point detection regime is adequate for the equal-path holographic interference, which is employed in our experiment.

We first recast classical holography with a simple in-line interferometric scheme, as sketched in Fig. 1(a). The beam from a source is divided into two daughter beams by a beamsplitter: one illuminates an object while the other travels freely, called object wave and reference wave, respectively. The two waves interfere at the recording material to form a hologram. Let x and x_0 be the transverse positions across the beam, $E_o(x)$ and $E_r(x)$ are the fields in the recording plane for the object wave and reference wave, respectively, and they satisfy

$$E_j(x) = \int h_j(x, x_0) E_0(x_0) dx_0, (j = o, r) \tag{1}$$

where $E_0(x_0)$ is the field distribution in the source plane. $h_j(x, x_0)$ stands for the impulse response function (IRF) for path $j = o, r$. Under the paraxial approximation, the IRF of the object wave and reference wave are written as

$$h_o(x, x_0) = \frac{k \exp(ikz_o)}{i2\pi\sqrt{z_{o1}z_{o2}}} \int dx' T(x') \exp\left[\frac{ik(x_0 - x')^2}{2z_{o1}} + \frac{ik(x' - x)^2}{2z_{o2}}\right], \tag{2a}$$

$$h_r(x, x_0) = H(x, x_0, z_r) \equiv \sqrt{\frac{k}{i2\pi z_r}} \exp(ikz_r) \exp\left[\frac{ik(x - x_0)^2}{2z_r}\right], \tag{2b}$$

respectively. k is the wave number of the beam. z_{o1} and z_{o2} are the distances from object to source and recording plane, respectively, and $z_o = z_{o1} + z_{o2}$; z_r is the diffraction length for the reference wave. For the convenience of theoretical treatment, we assume an transmissive object described by Function $T(x')$.

In holography, the object wave is usually much weaker than the reference wave. So the holographic pattern in the recording plane is dominated by the interference term $\langle E_r^*(x)E_o(x)\rangle$. When the temporal coherence condition is satisfied, that is $|z_r - z_o|$ is much less than the longitudinal coherence length of the beam, one arrives

$$\langle E_r^*(x)E_o(x)\rangle = \int dx_0' dx_0 h_r^*(x, x_0')h_o(x, x_0)\langle E_0^*(x_0')E_0(x_0)\rangle. \tag{3}$$

We consider three types of light sources in the spatial interference. The first source is a plane-wave coherent field, for which $\langle E_0^*(x_0')E_0(x_0)\rangle = \alpha^*\alpha$ is independent of transverse positions. Hence the first-order field correlation function can be factorized to be

$$\begin{aligned}&\langle E_r^*(x)E_o(x)\rangle = E_r^*(x)E_o(x)\\&= |\alpha|^2\sqrt{\frac{k}{i2\pi z_{o2}}}\exp[ik(z_o - z_r)]\int dx'T(x')\exp[ik(x-x')^2/(2z_{o2})],\end{aligned} \tag{4}$$

which records the holographic information of the object $T(x)$.

The second one is a thermal light source, shielded by a pinhole to improve the spatial coherence. This type of source was originally used in the first holography experiment[1]. In this case, Eq.(1) is reduced to $E_j(x) = h_j(x, x_0)E_0(x_0)\Delta x_0$, where x_0 and Δx_0 are the position and width of the pinhole, respectively. For simplicity, we assume $x_0 = 0$ and define $E_0(0)\Delta x_0 \equiv \beta$. Again, the first-order field correlation function is factorized to be

$$\begin{aligned}E_r^*(x)E_o(x) = &\left(\frac{k}{2\pi}\right)^{3/2}\frac{|\beta|^2\exp[ik(z_o - z_r)]}{\sqrt{iz_r z_{o1} z_{o2}}}\exp\left[\frac{ik(z_r - z_o)x^2}{2z_r z_o}\right]\\&\times\int dx'T(x')\exp\left[\frac{ik}{2Z}\left(x' - \frac{x}{1 + z_{o2}/z_{o1}}\right)^2\right],\end{aligned} \tag{5}$$

where the effective diffraction length is $Z = z_{o1}z_{o2}/z_o$. Since the longitudinal coherence length of true thermal light is very short, one must choose the equal-path configuration, i.e. $z_r = z_o$. So the quadratic phase factor term outside the integration disappears, and Eq. (5) has the similar form as Eq. (4). Especially when the object is far from the source, i.e. $z_{o1} >> z_{o2}$, the two equations become the same.

The last one is an incoherent thermal light source with an extended area, which satisfies $\langle E_0^*(x_0')E_0(x_0)\rangle = I_0\delta(x_0' - x_0)$. As has indicated above, this type of source is capable of performing incoherent interference under the certain conditions[2, 3]. Using Eq. (3) we

obtain

$$
\begin{aligned}
\langle E_r^*(x)E_o(x)\rangle &= I_0\int dx_0 h_r^*(x,x_0)h_o(x,x_0) \\
&= \frac{kI_0\exp[ik(z_o-z_r)]}{2\pi\sqrt{z_{o2}(z_r-z_{o1})}}\int dx' T(x')\exp\left[\frac{ik(x'-x)^2}{2Z'}\right],
\end{aligned}
\tag{6}
$$

where the effective diffraction length is $Z' = z_{o2}(z_r - z_{o1})/(z_r - z_o)$. Apparently, the scheme fails under the equal-path case because $Z' \to \infty$. However, the poor temporal coherence of a true thermal light source requires the equal-path condition in the interferometry. Hence this conflict results in conventional opinion that a true thermal light source with extended area is not appropriate for holographic interferometry. Recent experiment demonstrated that a pseudo-thermal light source associated with a laser having a long coherence time can accomplish this incoherent interference[2].

Quantum holography uses a two-photon entangled source and two-photon coincidence measurement[8]. A general two-photon entangled state can be written as $|\Psi\rangle = \int dx_1 dx_2 C(x_1,x_2)a_s^\dagger(x_1)a_i^\dagger(x_2)|0\rangle$, where $a_j^\dagger(j=s,i)$ are the photon creation operators for the two SPDC modes. $C(x_1,x_2) \sim \langle 0|E_{s0}^{(+)}(x_1)E_{i0}^{(+)}(x_2)|\Psi\rangle$ characterizes the two-photon wavepacket for the field operators $E_{s0}^{(+)}$ and $E_{i0}^{(+)}$ in the source plane. As shown in Fig. 1(b), while one signal photon passes through a holographic interferometer and the idler photon travels freely, the evolution of the field operator is given by Eq. (1) (with subscripts $j = so, sr, i$ instead of $j = o, r$). The signal field is divided into two parts, $E_{so}^{(+)}$ and $E_{sr}^{(+)}$, serving as the object and reference waves, respectively. The corresponding IRFs have been shown in Eq. (2)(with subscript so instead of o in Eq. (2a) and subscripts sr and i instead of r in Eq. (2b)).

Let $E_s^{(+)}(x)$ and $E_i^{(+)}(x)$ be the field operators of the signal and idler beams in the detector planes, respectively, the two-photon wavepacket in the observation planes has the form of $\langle 0|E_s^{(+)}(x_1)E_i^{(+)}(x_2)|\Psi\rangle$. The two-photon coincidence counting rate is $R(x_1,x_2) \propto \langle E_i^{(-)}(x_2)E_s^{(-)}(x_1)E_s^{(+)}(x_1)E_i^{(+)}(x_2)\rangle = |\langle 0|E_s^{(+)}(x_1)E_i^{(+)}(x_2)|\Psi\rangle|^2$. Because of $E_s^{(+)} = E_{so}^{(+)} + E_{sr}^{(+)}$, the rate consists of four parts: two parts are the two-photon intensities and the other two parts are the two-photon interference terms given by

$$
\begin{aligned}
&\langle E_i^{(-)}(x_2)E_{sr}^{(-)}(x_1)E_{so}^{(+)}(x_1)E_i^{(+)}(x_2)\rangle + c.c. \\
&= \langle\Psi|E_i^{(-)}(x_2)E_{sr}^{(-)}(x_1)|0\rangle \times \langle 0|E_{so}^{(+)}(x_1)E_i^{(+)}(x_2)|\Psi\rangle + c.c.,
\end{aligned}
\tag{7}
$$

which may include the holographic information. Note that this term defines the spatial

interference of two two-photon amplitudes and it is not involved in ghost interference and ghost imaging.

The two-photon wavepacket of Eq. (7) can be calculated by

$$\langle 0|E_j^{(+)}(x_1)E_i^{(+)}(x_2)|\Psi\rangle \propto \int dx_0' dx_0'' h_j(x_1, x_0')h_i(x_2, x_0'')C(x_0', x_0''), (j = so, sr), \tag{8}$$

where h_j is the IRF for beam $j = so, sr$. Particularly, h_{so} is given by Eq. (2a) with the corresponding distances z_{so}, z_{so1}, and z_{so2} to replace z_o, z_{o1}, and z_{o2}, respectively; $h_{sr} = H(x, x_0, z_{sr})$ and $h_i = H(x, x_0, z_i)$, where $H()$ is defined by Eq. (2b) and z_{sr} and z_i are the free traveling distances between source and detectors for the signal and idler beams, respectively. For simplicity, we consider an ideal two-photon entangled state at the source, satisfying $C(x_0', x_0'') = \delta(x_0' - x_0'')$. Equation (8) yields

$$\langle 0|E_j^{(+)}(x_1)E_i^{(+)}(x_2)|\Psi\rangle \propto \int dx_0 h_j(x_1, x_0)h_i(x_2, x_0), (j = so, sr). \tag{9}$$

This means the fact that the diffraction of the two-photon wavepacket is equivalent to the diffraction of one-photon which travels sequently through two paths with IRFs h_j and h_i. We thus obtain $\langle 0|E_{so}^{(+)}(x_0)E_i^{(+)}(x)|\Psi\rangle$ described by Eq. (2a) with z_{so1}, $z_{so2} + z_i$, and $z_{so} + z_i$ to replace z_{o1}, z_{o2}, and z_o, respectively. Also, it has $\langle 0|E_{sr}^{(+)}(x_0)E_i^{(+)}(x)|\Psi\rangle \propto H(x, x_0, z_i + z_{sr})$. An equivalent diagram is shown in Fig. 1(b), where one of the detectors in the two-photon coincidence measurement can act as a source. Therefore the two-photon holography can be easily understood in terms of one-photon case.

We first inspect the proposal by Abouraddy et al [8], where the bucket detection is employed for the beam passing through the interferometer. The coincidence counting rate in the bucket detection is $R_{bd}(x) = \int R(x, x_0)dx_0$. For the two-photon interference term, the integration of Eq. (7) gives the similar form of Eq. (6) with $z_o = z_i + z_{so}$, $z_r = z_i + z_{sr}$, and $Z' = (z_i + z_{so2})(z_i + z_{sr} - z_{so1})/(z_{sr} - z_{so})$. As a result, the bucket detector behaves as a spatially incoherent source in the equivalent diagram. Again, this scheme requires a certain difference between the object and reference paths. On the other hand, the longitudinal coherence of the two-photon interferometry is dominated by the coherence time of the pump beam. The scheme would be difficult or even impossible when the pump beam has a very limited coherence time such as a femtosecond pulse laser.

We now consider the point detection regime. According to the equivalent diagram, the similar result of Eq. (5) is obtained with $z_o = z_i + z_{so}$, $z_r = z_i + z_{sr}$, $z_{o1} = z_{so1}$, $z_{o2} = z_i + z_{so2}$

and $Z = z_{so1}(z_i + z_{so2})/(z_i + z_{so})$. At the equal path condition, $z_{so} = z_{sr}$, the quadrature phase factor in the interference term disappears.

Finally, we propose a coherent regime in the two-photon quantum holography, which can correspond to the plane-wave coherent field case in the classical holography. The detection system in the signal beam consists of a lens and a point detector, which is placed at the foci of the lens. The coherence is due to the fact that all the encoded photons to be detected have the same momentum. We have proved that the two-photon interference term (7) is the same as Eq.(4) with $z_{o2} = z_i + z_{so2}$[11].

In this work, we employ the point detection regime to accomplish quantum holographic imaging. The experimental setup is shown in Fig. 2. The entangled photon pairs are produced from SPDC in a $5 \times 5 \times 2\,\mathrm{mm}^3$ beta-barium-borate(BBO) crystal cut for type-I phase matching. The crystal is pumped by the second harmonic of a Ti:sapphire femtosecond laser (Mira-900 Coherent Inc.) with center wavelength 400 nm, and repetition rate 76 MHz. One of the down-converted beams, named the signal beam, passes through the interferometer where an object is set in the object arm, and then reaches detector D_1. The other down-converted beam, the idler beam, travels freely to detector D_2. Both the signal and idler photons are spectrally filtered by the interference filters of 10 nm bandwidth centered at 800 nm before arriving the single-photon detectors (Perkin-Elmer SPCMAQR-14). A time window of 4 ns is chosen to capture the coincidence counting.

Since a femtosecond pulse as the pump beam has very short coherence time (120fs), corresponding to the longitudinal coherence length of 36μm, we must use the equal-path interferometry. As a proof-of-principle experiment, the object to be holographically imaged is an amplitude grating of slit width $b = 200\,\mu$m and period $d = 400\,\mu$m, described by $T(x) = \sum_{n=-\infty}^{\infty} \mathrm{rect}[(x - nd - d/2)/b]$, where rect(u) is 1 for $|u| \leq 1/2$ and 0 for other values. In the near-field diffraction, the periodic object can be self-imaged at a certain distance (Talbot effect), characterized by the Talbot length $z_T = 2d^2/\lambda = 40\,\mathrm{cm}$ for $\lambda = 800\,\mathrm{nm}$[12]. So we can definitely know what we see in the holographic record.

For comparison, we first recast the one-photon holographic imaging experiment. In this scheme, the signal photon illuminates the holographic interferometer and is recorded by a scanning detector D_1 while the idler photon is employed as a trigger. To improve the spatial coherence, a single-slit aperture of width $100\,\mu$m is inserted in the signal beam. The grating is placed in the object arm of the interferometer at the same distance of $z_{o1} = z_{o2} = 40\,\mathrm{cm}$

to the single-slit and detector D_1. According to Eq. (5), the effective diffraction length is $Z = 20\,\mathrm{cm}$ (the half Talbot length), and the image magnification is two. So this will bring about the self-image of $T[(x-d)/2]$.

The experimental results are shown in Fig. 3. We first block the reference arm in the interferometer, and it comes back to the conventional Talbot self-imaging. We observe the self-image of the grating in Fig. 3(a), $|T[(x-d)/2]|^2$, which is phase-independent. Then we release the block to perform the holographic imaging, and the pattern $T[(x-d)/2]\cos\theta$ is phase-dependent, where phase θ is sensitive to the path difference $z_{so} - z_{sr}$. The in-phase image and out-of-phase image of the grating appear in Figs. 3(b) and 3(c), respectively, by adjusting the path difference carefully. If the single-slit aperture is taken away in the above two cases, the image patterns disappear as shown in Figs. 3(d) and 3(e).

Figures 3(d) and 3(e) tell us that the signal beam itself cannot accomplish the holographic imaging without the help of the single slit. We now turn to the two-photon nonlocal holographic imaging by rearrangement of the experimental setup in Fig. 2. Since the pump beam has poor temporal coherence, the equal-path condition must be applied to the two-photon interferometry. As has pointed out above, we must use the point detection scheme in two-photon quantum holography. The grating is placed at a distance $z_{so1} = 40\,\mathrm{cm}$ from detector D_1 and $z_{so2} = 15\,\mathrm{cm}$ from BBO crystal. The distance from BBO crystal to detector D_2 is $z_i = 25\,\mathrm{cm}$. Hence the effective diffraction length and the image magnification are the same as the one-photon case. In order to display the nonlocal feature in quantum holography, detector D_2 is scanned across the beam while D_1 is fixed in the two-photon coincidence measurement.

The experimental results in the two-photon holography are presented in Fig. 4. Again, Fig. 4(a) shows the self-image of the grating when the reference arm of the interferometer is blocked. This is the two-photon Talbot self-imaging in the ghost interference scheme, reported recently by Song et al[12]. In this case, the interference-diffraction pattern is phase-independent. When the block is moved away, the in-phase image and out-of-phase image are shown in Figs. 4(b) and 4(c), respectively. Obviously, these patterns in Fig. 4 match better with the corresponding ones in Fig. 3 for the one-photon case. If we use a bucket detector to replace the point detector in the signal photon detection, both in-phase and out-of-phase image patterns disappear, as shown in Figs. 4(d) and 4(e).

In summary, we have demonstrated experimentally the spatial interference effect of two

two-photon amplitudes given by Eq. (7), which is the origin of quantum holography. We have analyzed three schemes of quantum holography using a two-photon entangled source: the point detection, the coherent detection and the bucket detection. The first two are appropriate for the equal-path configuration while the last, on contrary, must sustain a certain optical path difference in the interferometry. Our experiment has demonstrated the two-photon quantum holographic imaging in the point detection regime through the two photon correlation measurement, although the individual detection of the signal and idler photons do not show any interference pattern. To make a true hologram, however, it needs to develop two-photon recording material. Similar to ghost interference and ghost imaging, the quantum holography reveals nonlocality of quantum entanglement. Ghost interference and ghost imaging testify the EPR nonlocal correlation in momentum and in position, respectively[6, 7]. In quantum holography, however, a pair of non-commutable physical quantities, the amplitude and phase of the field, can be nonlocally measured through the two-photon entanglement. Therefore our experiment on quantum holography may provide a more authentic version to understand EPR paradox.

This work was supported by the National Natural Science Foundation of China, Project Nos. 11174038, 11047004 and 10825416, and the National High Technology Research and Development Program of China, Project Grant No. 2011AA120102, and the Fundamental Research Funds for the Central Universities.

[1] D. Gabor, Nature, **161**, 777 (1948).

[2] S. H. Zhang, L. Gao, J. Xiong, L. J. Feng, D. Zh. Cao, and K. Wang, Phys. Rev. Lett. **102**, 073904 (2009).

[3] S. H. Zhang, Sh. Gan, D. Zh. Cao, J. Xiong, X. Zhang, and K. Wang, Phys. Rev. A **80**, 031805R (2009).

[4] A. Einstein, B. Podolsky, and N. Rosen, Phys. Rev. **47**, 777 (1935).

[5] A. V. Belinskii and D. N. Klyshko, JETP **78**, 259 (1994).

[6] D. V. Strekalov, A. V. Sergienko, D. N. Klyshko, and Y. H. Shih, Phys. Rev. Lett., **74**, 3600 (1995).

[7] T. B. Pittman, Y. H. Shih, D. V. Strecalov, and A. V. Sergienko, Phys. Rev. A, **52**, R3429

(1995).

[8] A. F. Abouraddy, B. E. A. Saleh, A. V. Sergienko and M. C. Teich, Opt. Express, **9**, 498 (2001).

[9] A. Einstein, in *The Born-Einstein Letters* (Walker, New York, 1971), p. 158, translated by I. Born.

[10] A. F. Abouraddy, P. R. Stone, A. V. Sergienko, B. E. A. Saleh, and M. C. Teich, Phys. Rev. Lett. **93**, 213903 (2004).

[11] Supplemental material.

[12] X. B. Song et al, Phys. Rev. Lett. **107**, 033902 (2011).

Figure captions:

Fig. 1 Sketches of (a) one-photon classical holography and (b) two-photon quantum holography. BS and M are beamsplitter and mirror, respectively. In (a), CS, PS, and InCS are the plane-wave coherent source, point source, and spatially incoherent source, respectively. RM is the recording material. In (b), CD, PD, BD are the coherent detection, point detection, and bucket detection, respectively.

Fig. 2 Experimental setup of two-photon holographic imaging. Two beamsplitters, BS_1 and BS_2, and two mirrors, M_1 and M_2, form an interferometer. NF is the neutral-density filter, and D_1 and D_2 are two detectors.

Fig. 3 Experimental results of one-photon holographic imaging. CC is the coincidence counting when detector D_1 is scanned and detector D_2 is as a trigger. (a) the self-image of the grating when the reference path of the interferometer is blocked; (b) and (c) are respectively the in-phase and out-of-phase images when the reference path of the interferometer is opened. When the single-slit aperture in the signal beam is taken away in the cases of (b) and (c), the self-images disappear as shown in (d) and (e), respectively.

Fig. 4 Experimental results of two-photon holographic imaging. CC is the coincidence counting when detector D_2 is scanned and detector D_1 is fixed. (a)-(c) the same as in Fig. 3. When the bucket detector is employed in D_1 in the cases of (b) and (c), the self-images disappear as shown in (d) and (e), respectively.

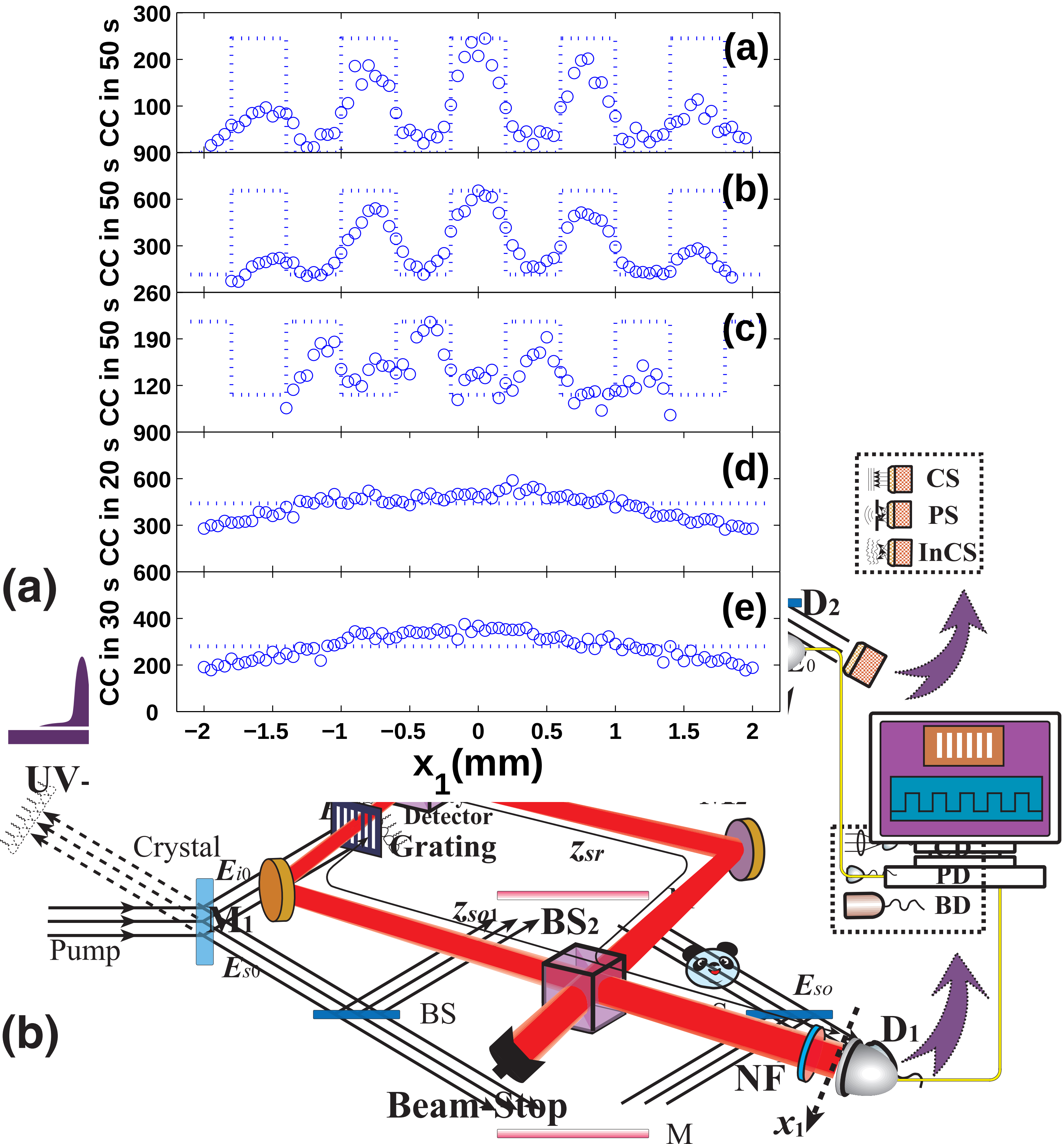
(a)
(b)
(c)
(d)
(e)
CC in 50 s
CC in 50 s
CC in 50 s
CC in 20 s
CC in 30 s
x1(mm)
CS
PS
InCS
D2
UV-
Crystal
Detector
Grating
Ei0
Zsr
Zso1
BS2
M1
Pump
Es0
BS
Eso
D1
NF
Beam-Stop
x1
M
PD
BD

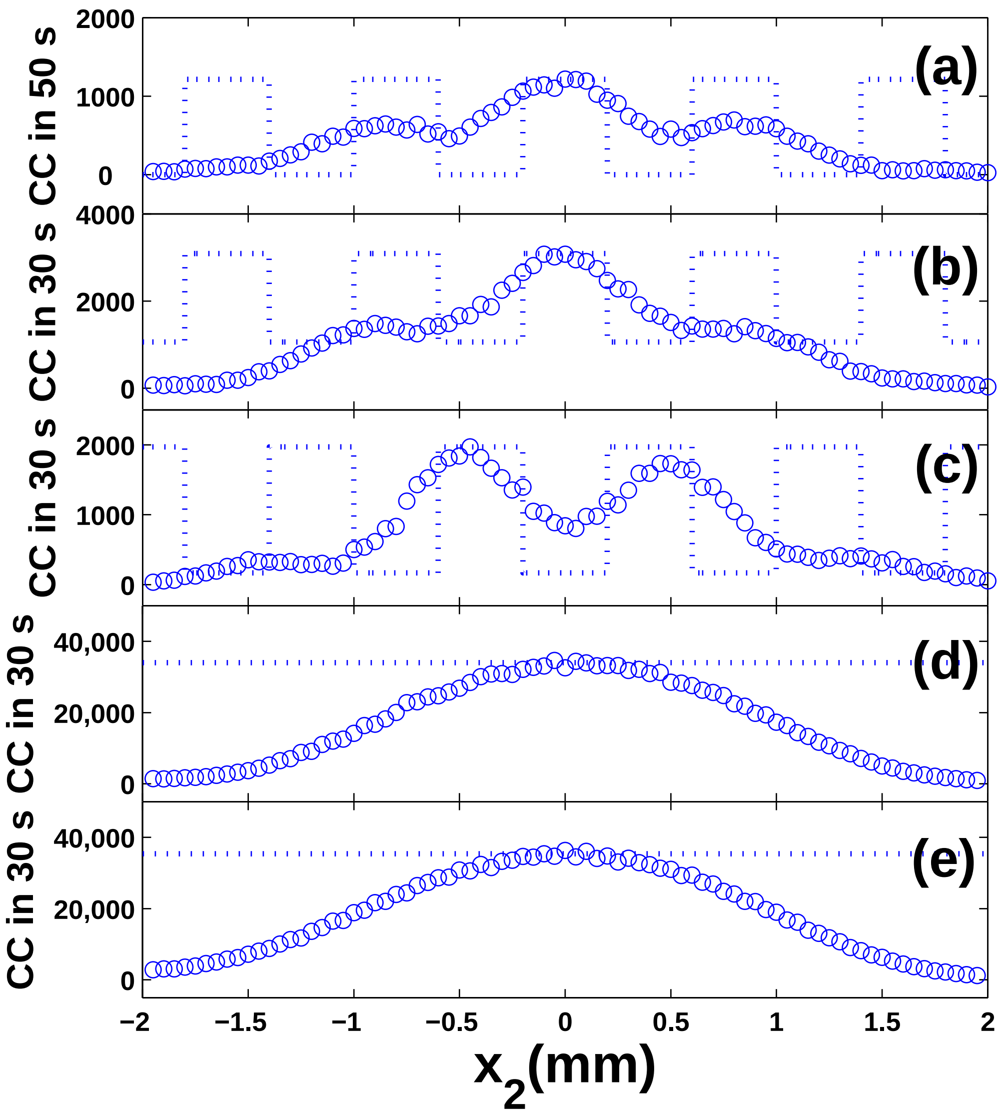

CC in 50 s
CC in 30 s
CC in 30 s
CC in 30 s
CC in 30 s
2000
1000
0
4000
2000
0
2000
1000
0
40,000
20,000
0
40,000
20,000
0
(a)
(b)
(c)
(d)
(e)
−2
−1.5
−1
−0.5
0
0.5
1
1.5
2
x2(mm)